

Inhibition curves in Human Serum

Chiara

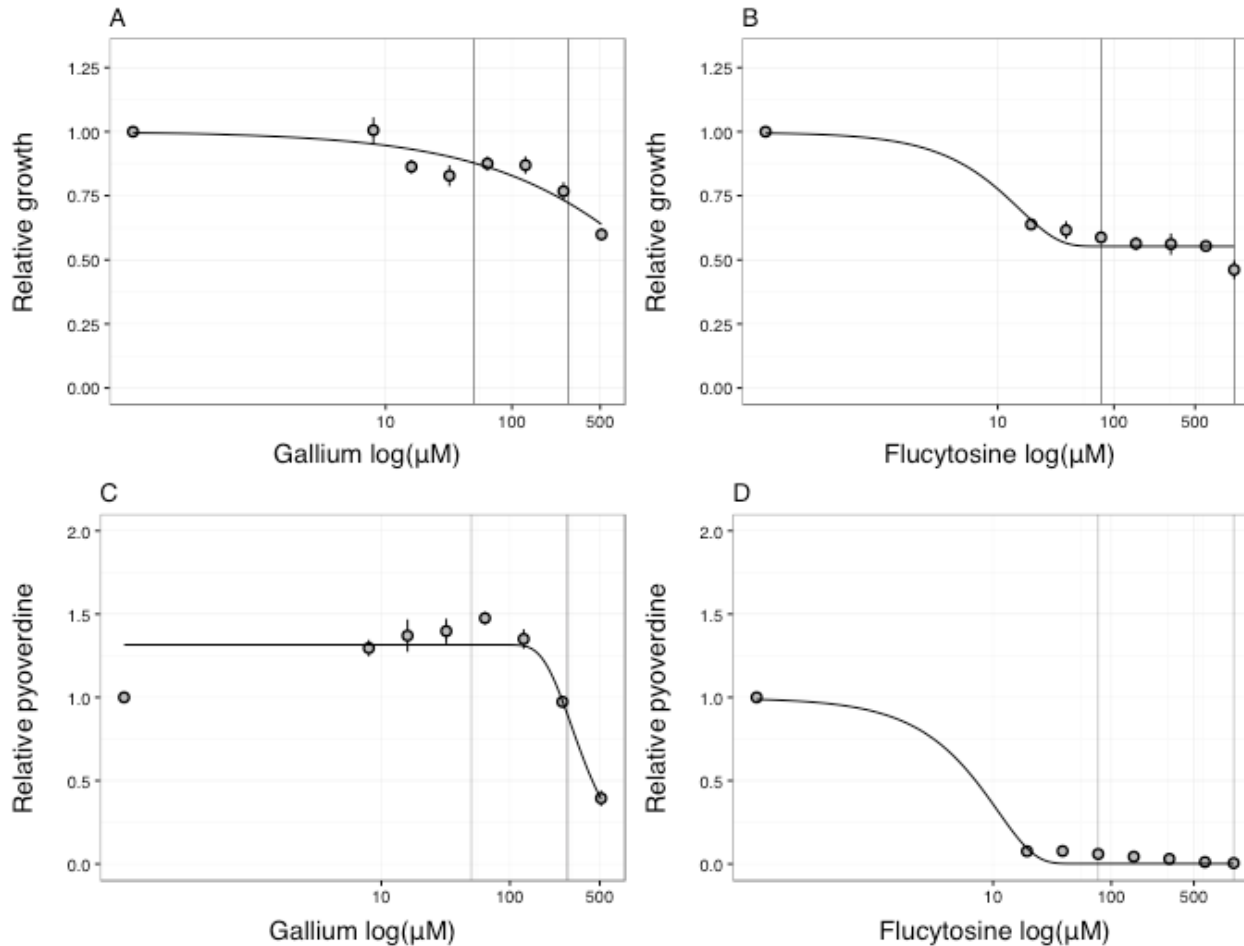


Fig. 1 Gallium and Flucytosine inhibition curves in Human Serum (HS). Growth and pyoverdine production of *P. aeruginosa* PAO1 subjected to a range of antibacterial concentrations were measured after 24 h in Human Serum. Data are shown as a ratio of values at concentration zero. Error bars denote standard errors of the mean. Vertical lines indicate the concentrations used in the experimental evolution. (A) Dose-growth response curve of PAO1 under gallium treatments was fitted with a 2-parameters Weibull function (lack of fit test $p=0.01$); growth reduction in response of flucytosine was fitted with a 4-parameters Gompertz function (lack of fit test $p=0.008$). (B) Changes in pyoverdine expression can be modeled with a 3-parameter Weibull function (lack of fit test $p=0.000$) in response to gallium and with a 4-parameters Gompertz (lack of fit test $p=0.000$) under flucytosine treatments.

Chiara

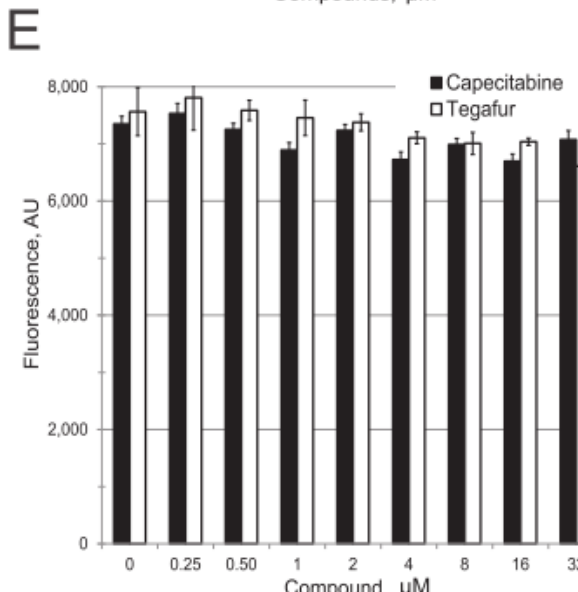
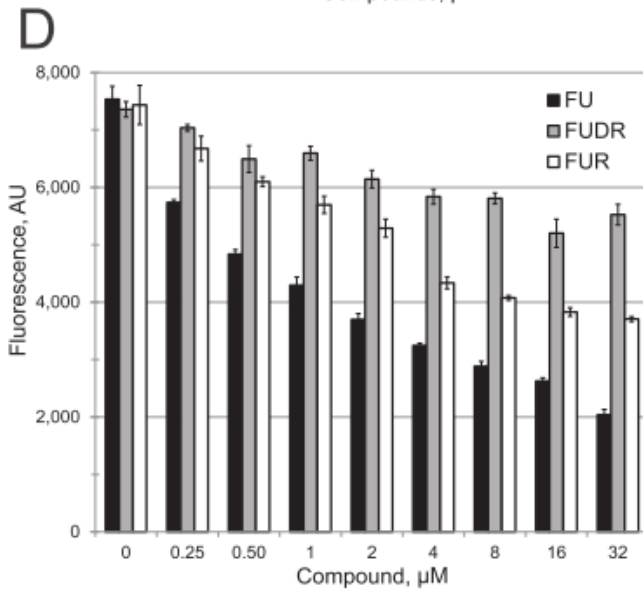
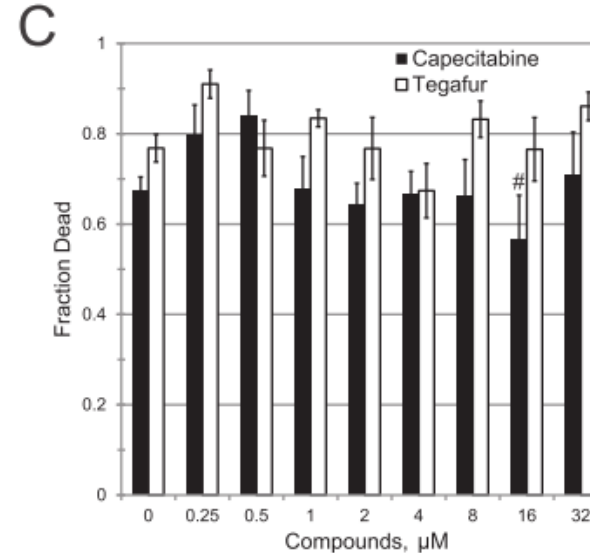
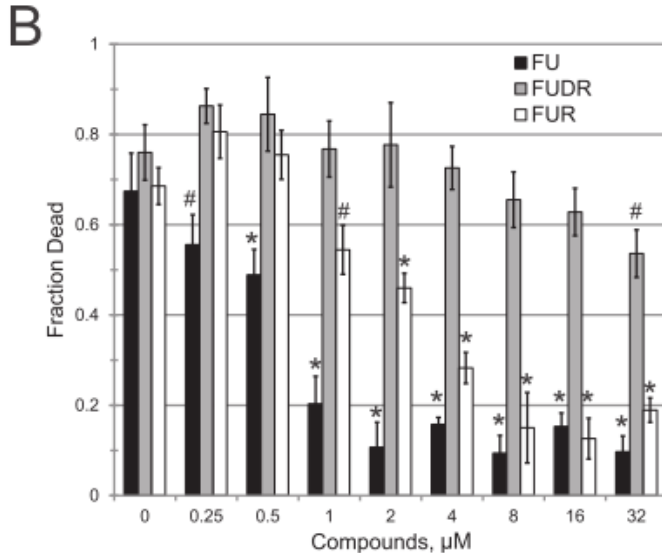


FIG 3 5-Fluorouracil-based therapeutics interfere with pyoverdine biosynthesis. (A) Schematic of 5-fluorouracil metabolism in *P. aeruginosa*. The diagram shows the complex relationships between pyrimidine analogs. OMP, orotate monophosphate. Compounds tested with 5-fluorinated derivatives are indicated in bold. (B and D) Dose-response curves of *C. elegans* exposed to *P. aeruginosa* under liquid killing conditions in the presence of 5-fluorouracil (FU; black), 5-fluorodeoxyuridine (FUDR; gray), or 5-fluorouridine (FUR; white). Killing results (B) and pyoverdine fluorescence after 24 h of infection (D) are shown. (C and E) Dose-response curves of *C. elegans* exposed to *P. aeruginosa* in the presence of capecitabine (black) or tegafur (white). Killing results (C) and pyoverdine fluorescence after 24 h of infection (E) are shown. Statistical significance: *, $P < 0.01$; #, $P < 0.05$ (based on Student's *t* test). At least three biological replicates were done for each compound. Data from a representative replicate are shown.

Enrique

- Mykland P, Tierney L, Yu B (1995) Regeneration in Markov chain samplers. *Journal of the American Statistical Association* 90:233-241, Figure 1

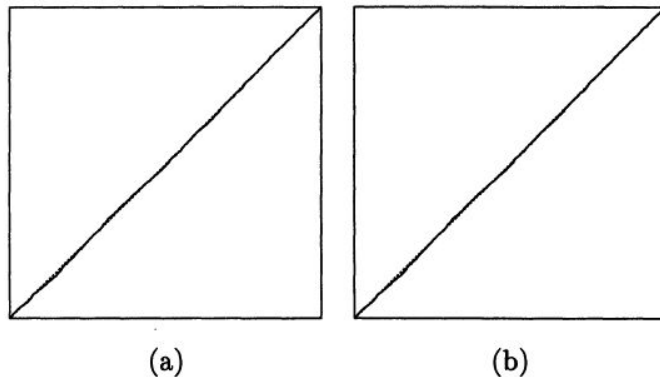


Figure 1. SRQ Plots of T_i/T_n (Vertical Axes) Against i/n (Horizontal Axes) for the Gibbs Sampler (a) and an Alternating Gibbs/Independence Sampler (b) for the Pump Failure Data Based on Runs of Length 5,000. Lines through the origin with unit slope are shown dashed; axis ranges are from 0 to 1 for all axes.

Roeder K (1994) DNA fingerprinting: A review of the controversy (with discussion). *Statistical Science* 9:222-278, Figure 4

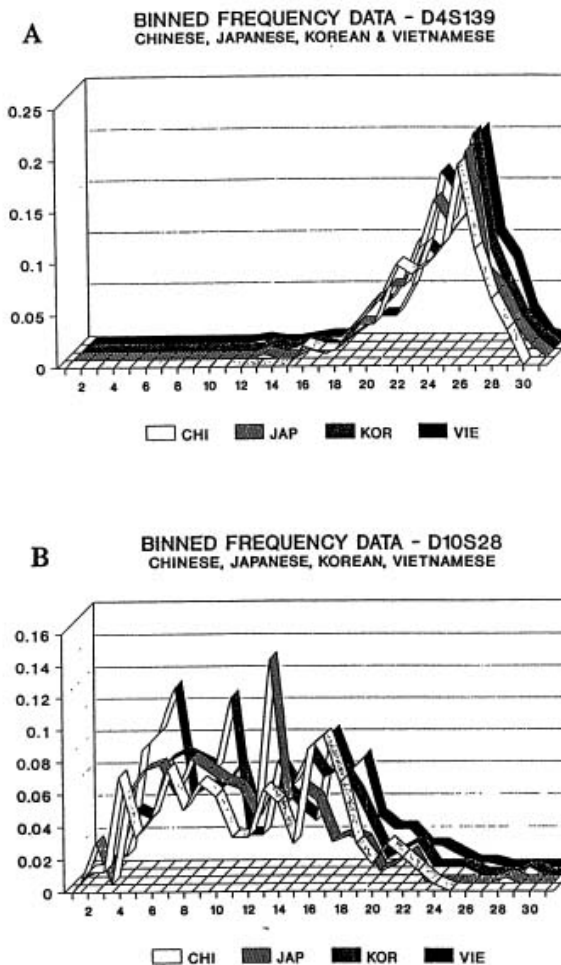


FIG. 4. Fixed bin distribution (histogram) for two loci and four Asian subpopulations (used with permission from John Hartmann): the boundaries of the 30 bins (vertical axis) are determined by the FBI; these bins are not of equal length. Sample sizes (numbers of individuals) for Chinese, Japanese, Korean and Vietnamese are 103, 125, 93 and 215 for D4S139 and 120, 137, 100 and 193 for D10S28. The horizontal axis is the bin number; bins are not of equal length.

Enrique

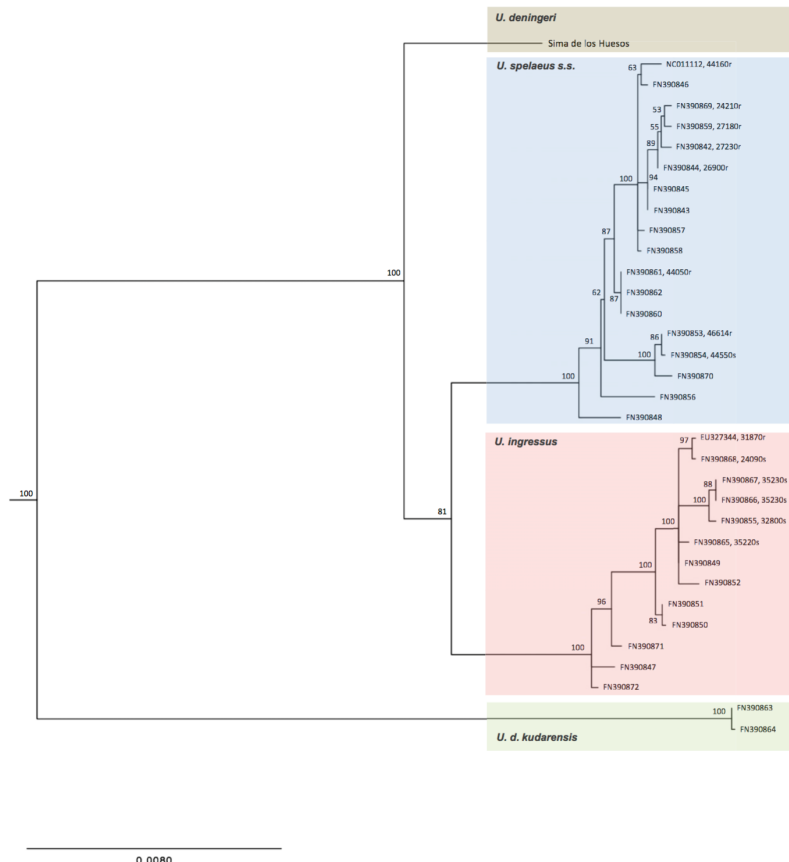


Fig. 3. Phylogenetic position of *U. deningeri* within Late Pleistocene cave bears. ML reconstruction of cave bear relationships is shown. Numbers on branches represent bootstrap support. The tree is rooted with five brown bear sequences as outgroup (branch not depicted). Age of the samples is provided in brackets where known (r and s denote radiocarbon and stratigraphic dates, respectively).

- Dabney, Jesse; Knall, Michael; Glocke, Isabell. Complete mitochondrial genome sequence of a Middle Pleistocene cave bear reconstructed from ultrashort DNA fragments. 2013. Proceedings of the National Academy of Sciences, Volume 110, 39, pg. 15758 - 15763

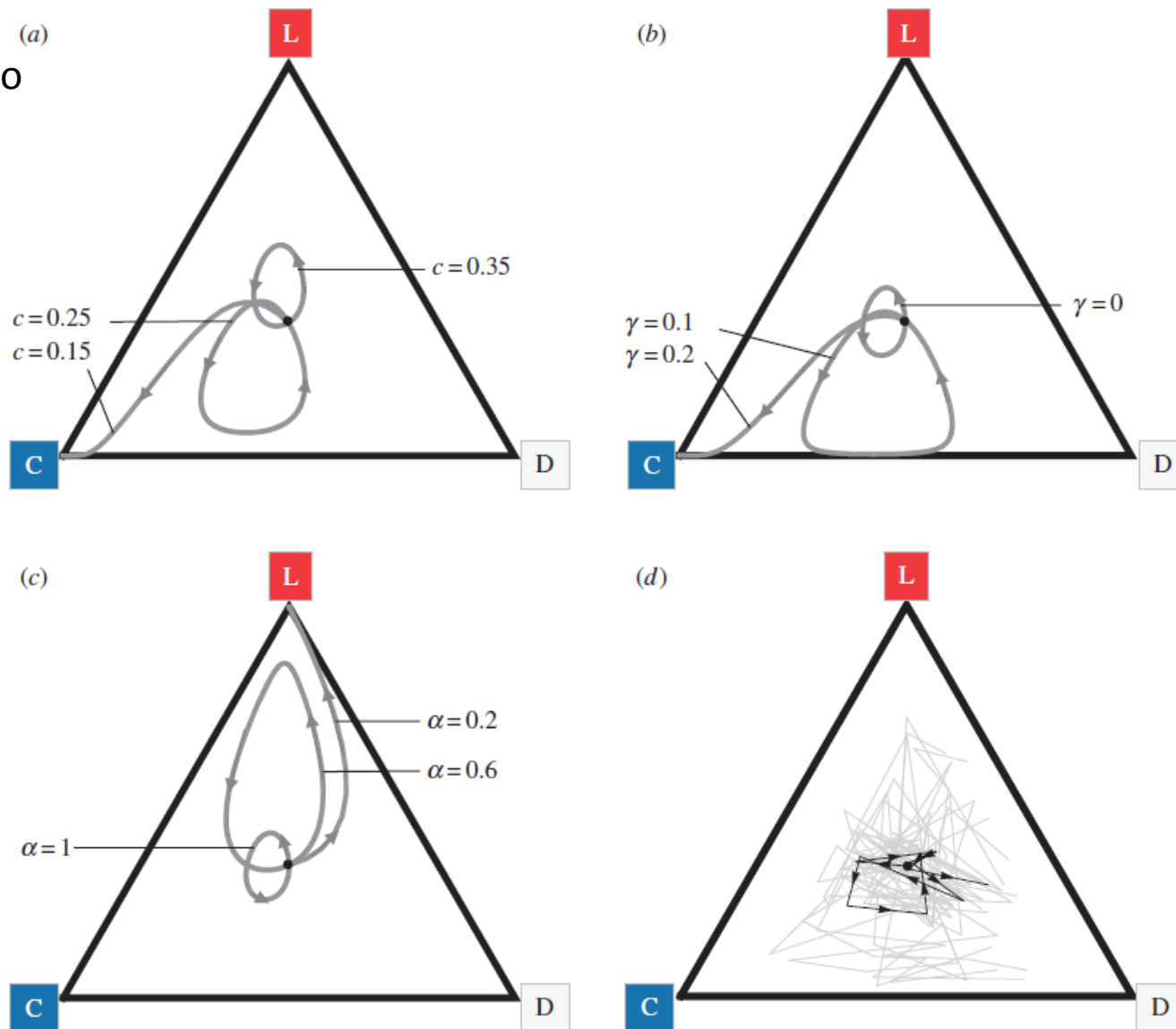


Figure 2. Maintenance of cooperation and diversity in three-strain communities. Triangular plots of deterministic numerical analyses, showing that in communities consisting of a cooperator (C), a defector (D) and a loner (L), rock–paper–scissors dynamics arise when: (a) the cost c of siderophores is sufficiently high; (b) the proportion γ of siderophores retained by the cooperator for personal use is low and (c) the proportion α of siderophores being shared in local neighbourhoods is high. All analyses start with strain types at equal frequency (one-third, shown by the black circle) and, unless otherwise specified, parameters are $c = 0.3$, $b = 0.7$, $\alpha = 1$, $\gamma = 0$, $n = 5$, $\mu = 0$. (d) Experiments with three-strain communities of *Pseudomonas* bacteria recover the theoretically predicted rock–paper–scissors dynamics (grey lines show 12 independent replicates; black line shows the mean over 10 days of experimental evolution).

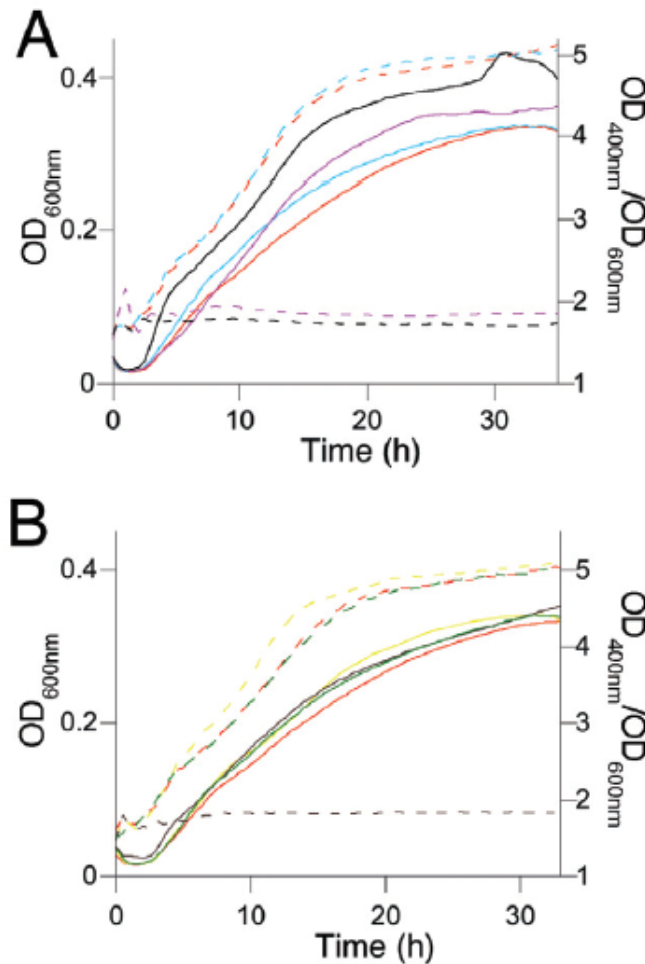
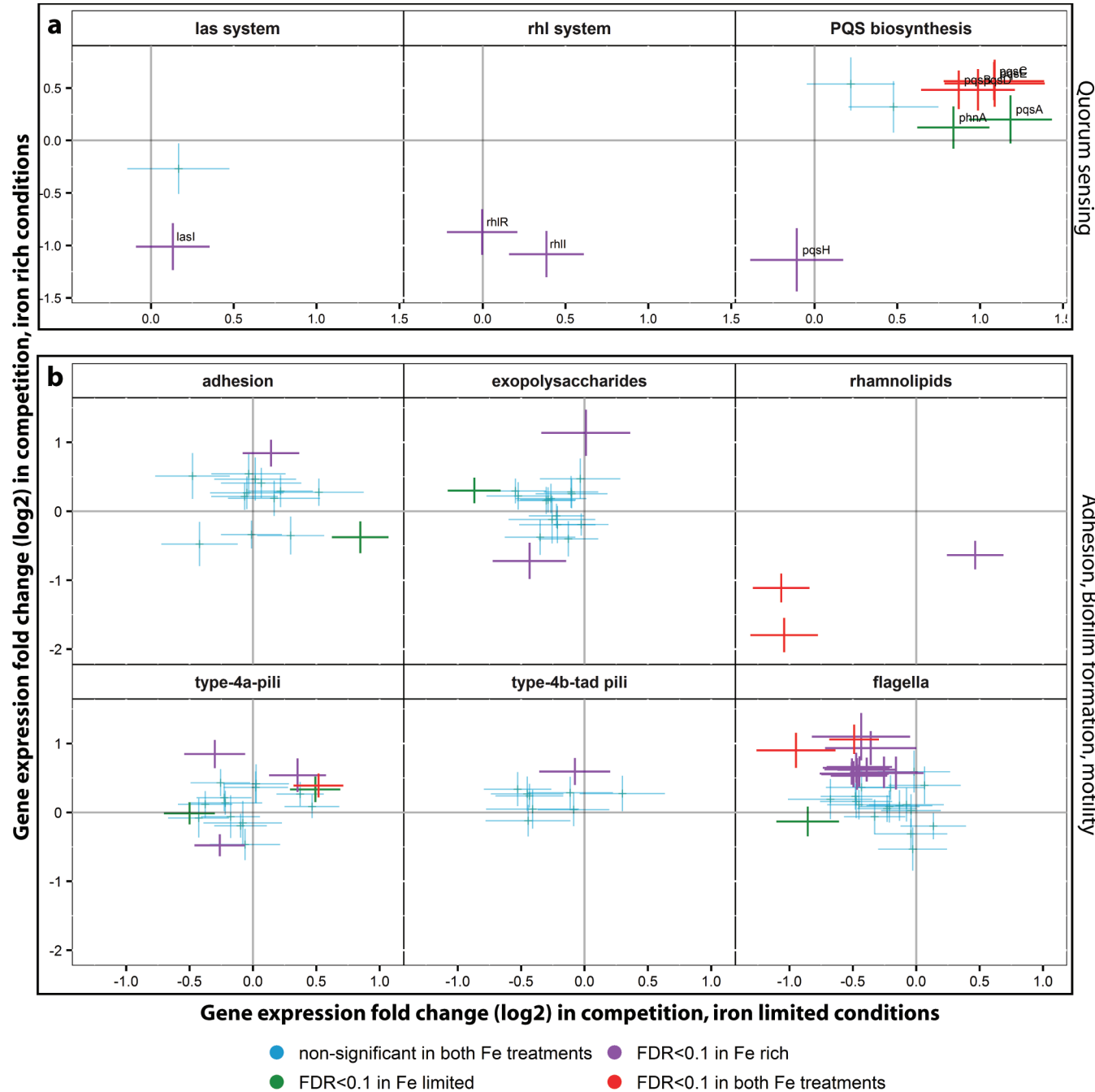
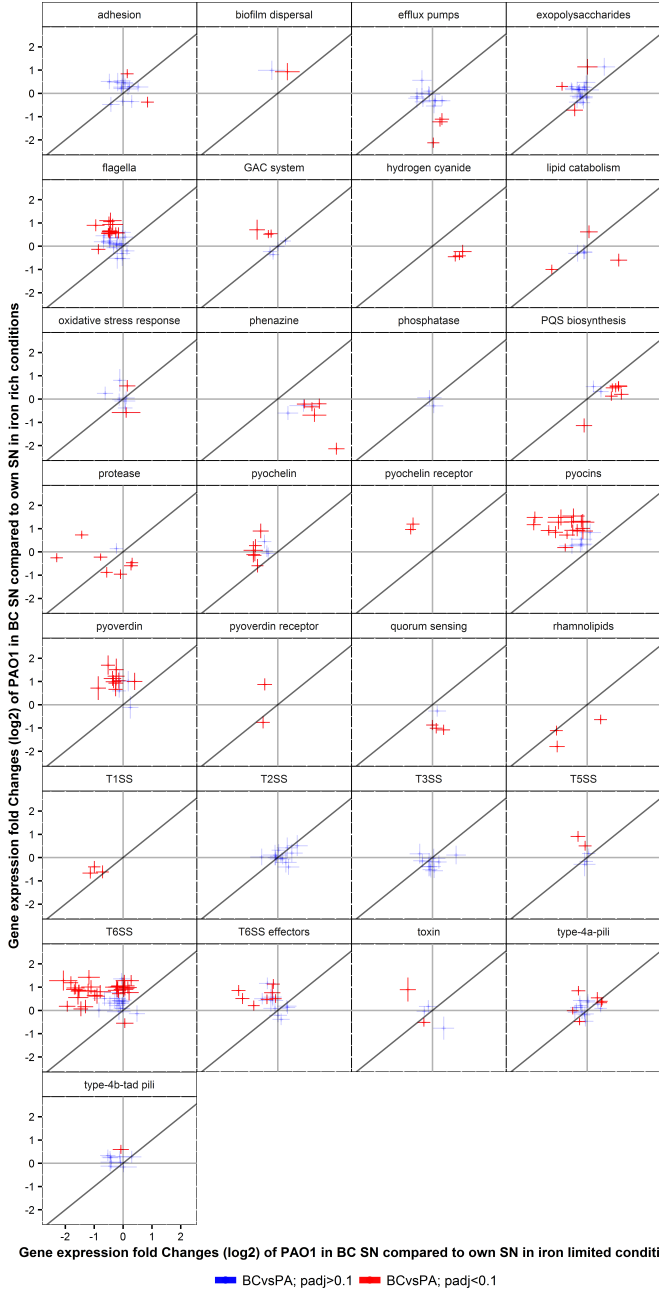


Fig. 1. Effect of fusion proteins of eYFP with PvdA (A) and of mCHERRY with PvdQ (B) on bacterial growth and PVDI production. Bacteria were washed in iron-depleted succinate media to remove iron from LB media. Fresh minimal media were then inoculated with these bacteria and distributed into a 96-well plate. The growth (solid lines in panels A and B) and PVDI production (dashed lines in panels A and B) were monitored over time by OD₆₀₀ and OD₄₀₀ measurements. Panel (A) presents the measurements for PAO1 (red), PAO1-pvdA (black), yfp-pvdA (pink), and pvdA-yfp (blue) and panel (B) for PAO1 (red), PAO1-pvdQ (brown), mcherry-pvdQ (green), and pvdQ-mcherry (yellow). These measurements were performed every 30 min in a Tecan microplate reader with shaking and incubation at 30°C. Each curve represents a mean derived from six replicates. PVDI production (OD₄₀₀) at a given time was normalized by the corresponding bacterial-growth reading (OD₆₀₀).

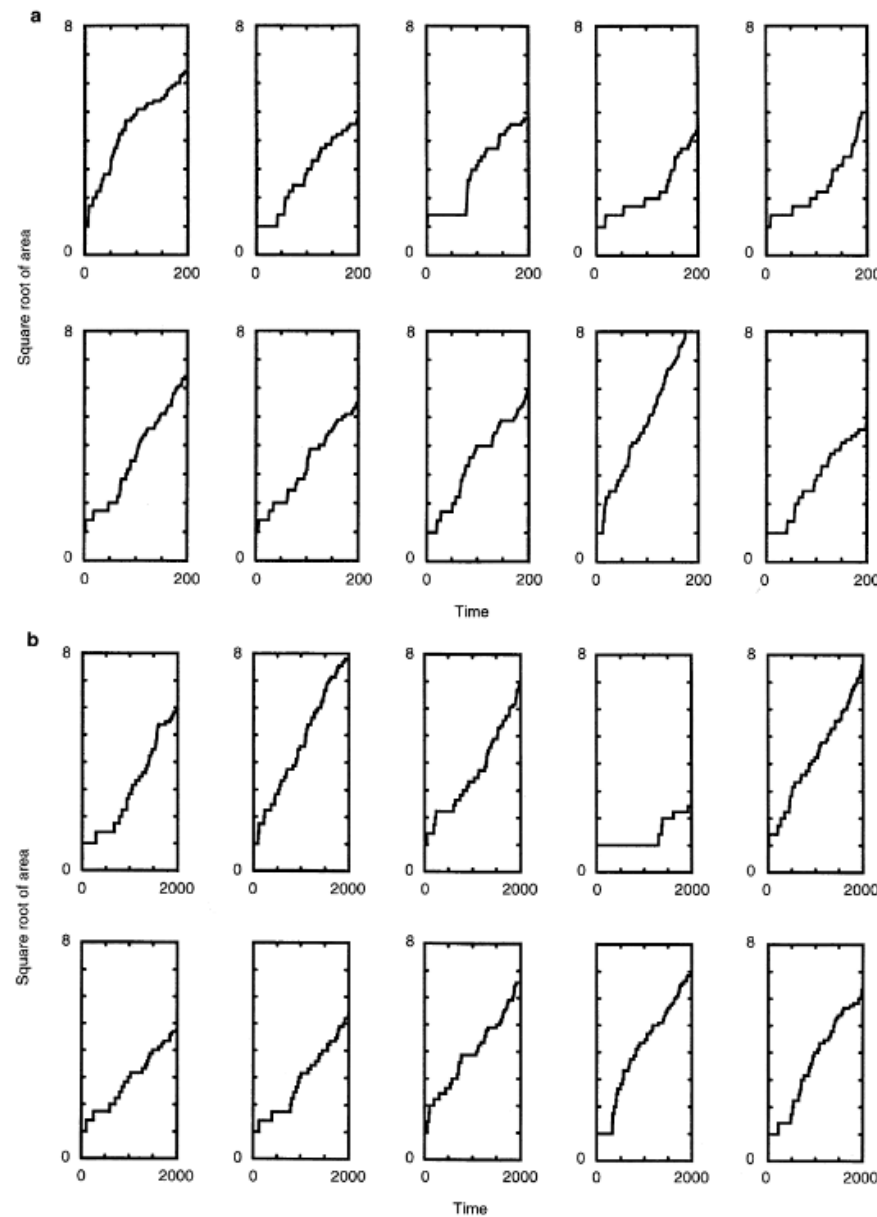
Anne



Anne



Felix



Reasoning: Axes are not declared very well. Figure does not contain any caption concerning the meaning/interpretation, forcing reader to look through the text in order to find out what the figure means.

Felix

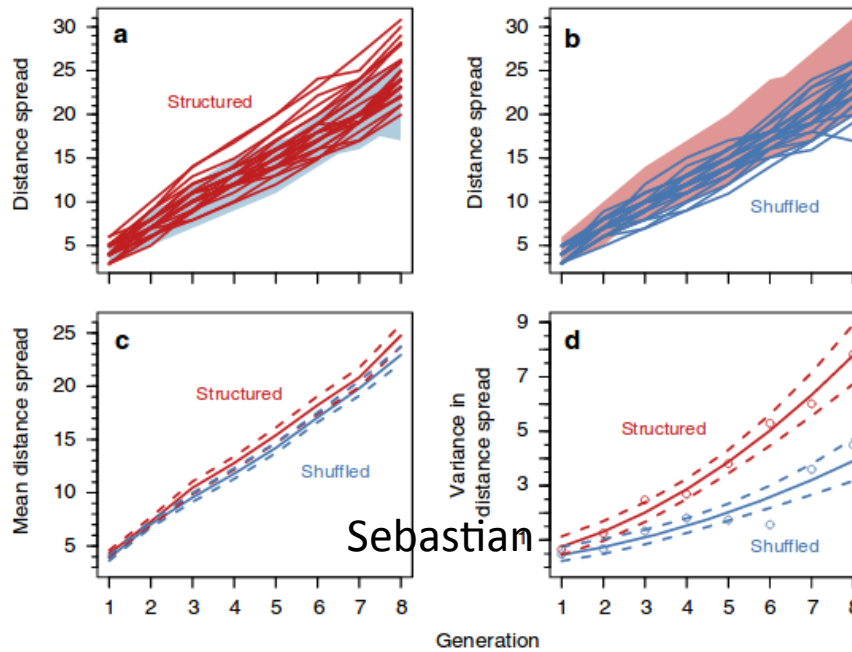
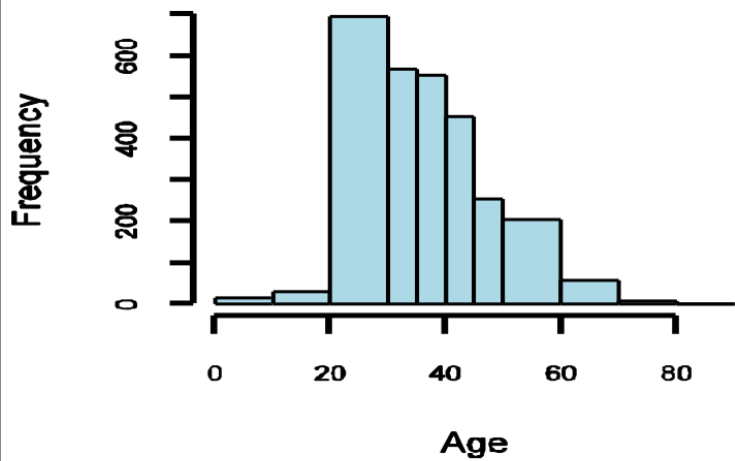


Figure 1 | Speed and variability of structured and shuffled range expansions. Experimental results of range expansions with structured ($n=28$) and shuffled ($n=29$) populations initiated from a single well-mixed source population. (a,b) Distances spread in each treatment. The lines show data for individual replicates whereas the shaded regions show the observed range of distance spread in the other treatment for reference. (c) Mean distance spread through time for each treatment (solid lines) and sample estimated 95% confidence intervals (dashed lines). (d) Model-estimated variances for each treatment with 95% confidence intervals. The observed variances for each treatment are shown as points. In all panels the structured treatment is shown in red and the shuffled treatment in blue. Spatial evolution resulted in a higher mean expansion speed (parametric bootstrap, treatment by generation interaction: $P=0.0137$) and higher variance in expansion speeds (likelihood ratio test, treatment by generation interaction: $P=1.93 \times 10^{-5}$).

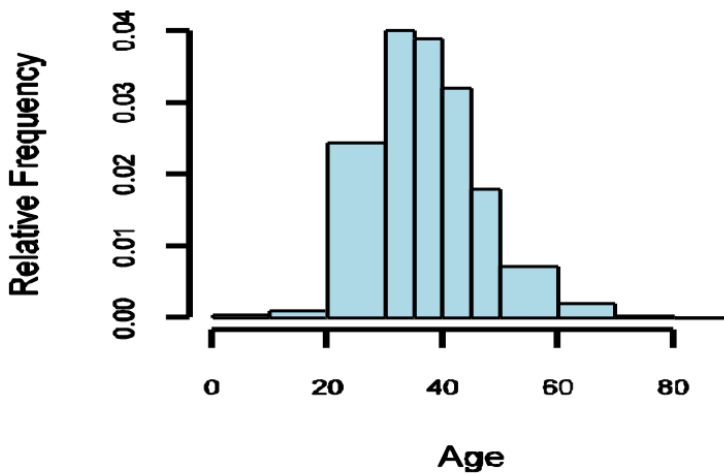
Reasoning: Axes well annotated. Good efforts have been made to ensure figure is visually well interpretable (i.e. separation of results for plot A and B, while keeping results of other plot as reference (shaded area's)). Clear explanation in the figure caption.

Hoda

Distribution of Ages



Distribution of Ages



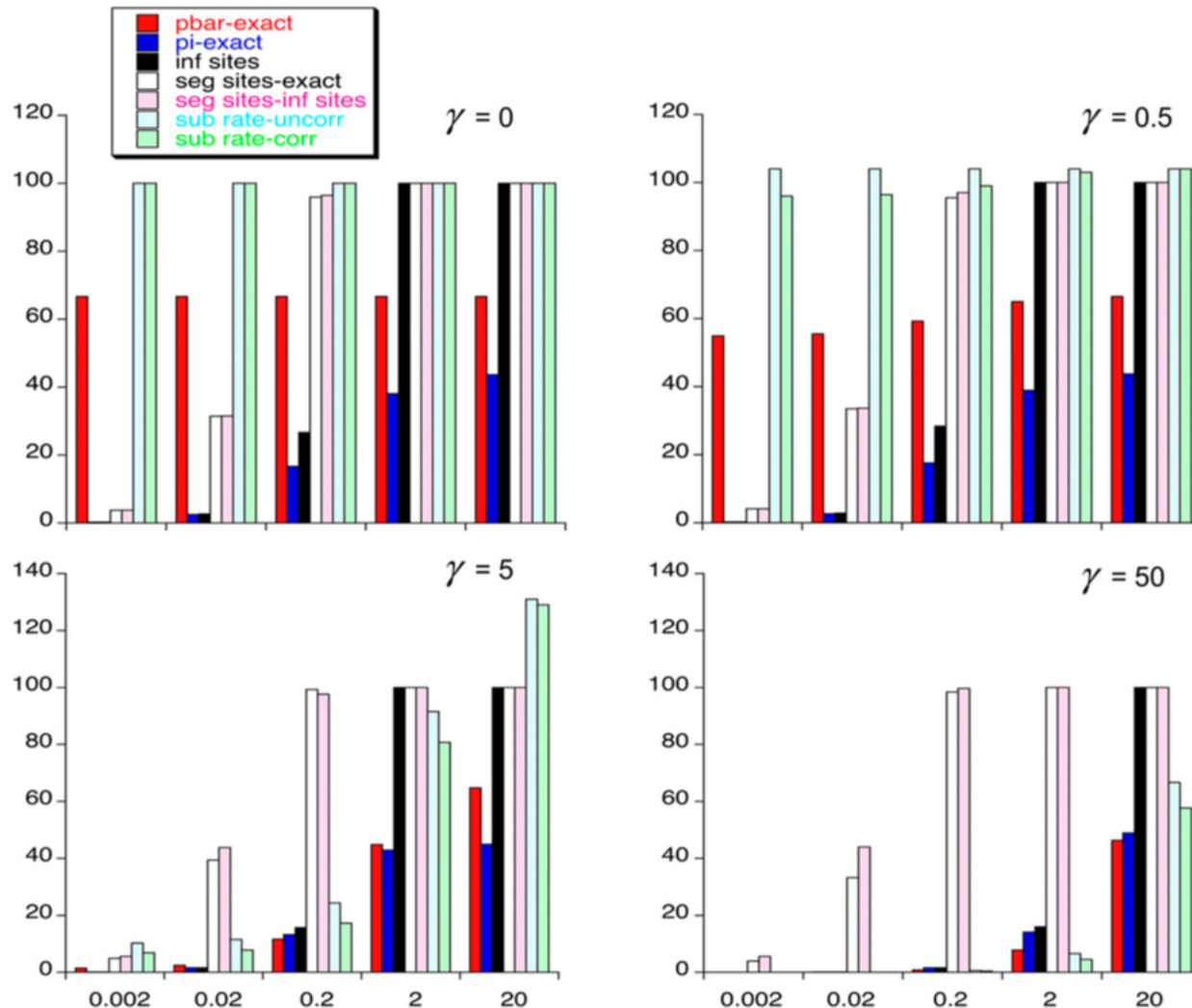
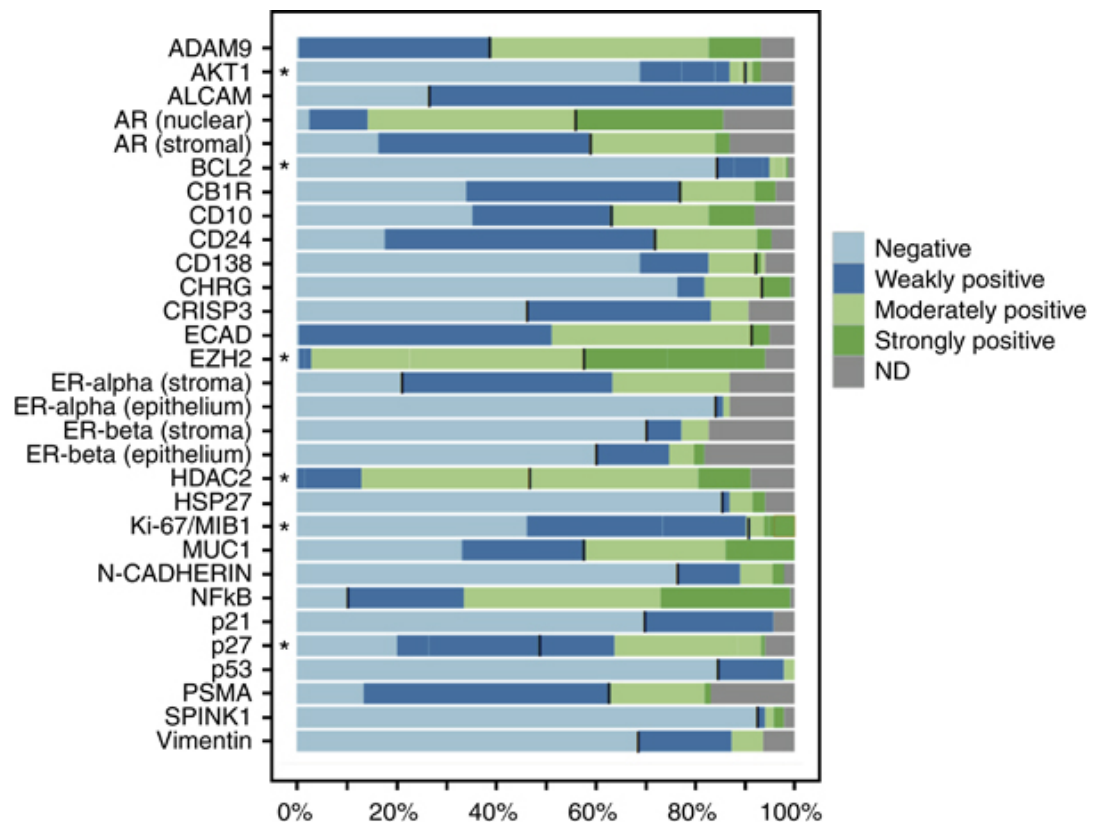
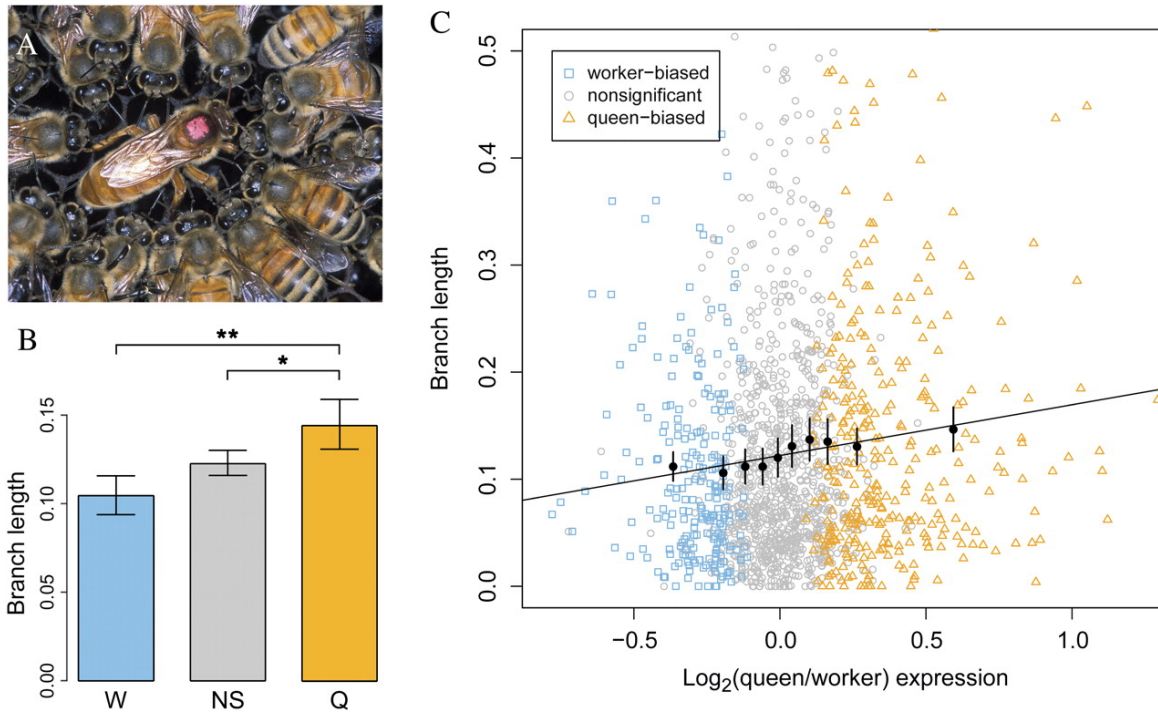


Figure 1 The vertical bars are the values (in percentages) of the mean frequency of A_1 , \bar{p} (red), π from Equation 10b (blue), π as given by the infinite sites model (black), the proportion of segregating sites from Equation 9 (white), the proportion of segregating sites under the infinite sites model (pink), the uncorrected rate of substitution relative to neutrality (light blue), and the corrected rate of substitution relative to neutrality (green).



Frequencies of immunohistochemically detected expression of selected prognostic markers in primary prostate carcinomas.
 Markers labelled with an asterisk were recorded as immunoreactive scores and summarised for easier visualisation (IRS 0: negative, IRS 1–3: weakly positive, IRS 4–8 moderately positive, IRS>8: strongly positive). Black bars indicate the cut-off used for dichotomising the variable for Cox regression analysis. Abbreviation: ND: non determined/missing data



Caste-biased gene expression is linked to protein evolutionary rate in *Apis mellifera*.

(A) *Apis mellifera* workers surround a queen. (B) *Apis mellifera* evolutionary rates (branch lengths in amino acid substitutions per site) differ significantly among genes with worker-biased expression (W), nonsignificant bias (NS), and queen-biased expression (Q; Kruskal–Wallis P = 0.0019). Means with 95% confidence intervals are plotted, and significant differences are indicated (*P < 0.05 and **P < 0.01 pairwise Mann–Whitney U test with Bonferroni correction). (C) Log₂-transformed ratios of queen-to-worker gene expression are correlated with *A. mellifera* evolutionary rates (Spearman's rank correlation rs = 0.096, P = 0.0002). A linear model best-fit line is plotted, and mean values for 10 equally sized bins of genes are shown as black dots with 95% confidence intervals. Outliers beyond the scaled axes contribute to plotted means and confidence intervals.

Sebastian Schmidt

